Amplitude Scaling of Wave Packets in Turbulent Jets

Luigi A. Antonialli* and André V. G. Cavalieri†
Aeronautics Technological Institute, 12228-900 São José dos Campos, Brazil
Oliver T. Schmidt‡
University of California, San Diego, San Diego, California 92093
Tim Colonius§
California Institute of Technology, Pasadena, California 91125
Peter Jordan¶
University of Poitiers, 86000 Poitiers, France
Aaron Towne**
University of Michigan, Ann Arbor, Michigan 48109
and
Guillaume A. Brès††
Cascade Technologies, Palo Alto, California 94303

https://doi.org/10.2514/1.J059599

This paper studies the amplitude of large-scale coherent wave-packet structures in jets, modeled by the parabolized stability equations (PSEs). Linear PSEs can retrieve the shape of the wave packets, but linearity leads to solutions with a free amplitude, which has traditionally been obtained in an ad hoc manner using limited data. We systematically determine the free amplitude as a function of frequency and azimuthal wave number by comparing the fluctuation fields retrieved from PSEs with coherent structures educed from large-eddy simulation data using spectral proper orthogonal decomposition. The wave-packet amplitude is shown to decay exponentially with the Strouhal number for axisymmetric and helical modes at both Mach numbers considered in the study: 0.4 and 0.9. Analytical fit functions are proposed, and the scaled wave packets provide reasonable reconstructions of pressure and velocity spectra on the jet centerline and lip line over a range of streamwise positions.

Nomenclature

A	=	scaling factor
$a(\xi)$	=	hydrodynamic wave number
a_j	=	amplitude captured my mode j
C_a, C_b	=	exponential function coefficients
c_0	=	ambient sound speed
D	=	jet diameter
E	=	error
f, g	=	generic functions
M	=	Mach number
m	=	azimuthal wave number
P	=	pressure fluctuation
$\boldsymbol{q}$	=	flow variables
$\hat{\boldsymbol{q}}_{\text{pse}}$	=	fluctuation flowfield calculated from parabolic stability equations in the frequency domain
$\hat{\boldsymbol{q}}_{\text{spod}}$	=	flow fluctuations for the leading spectral proper orthogonal decomposition in the frequency domain
$\boldsymbol{q}'$	=	flow fluctuations in the time domain
$\bar{\boldsymbol{q}}$	=	time-averaged component of $\boldsymbol{q}$
$\tilde{\boldsymbol{q}}$	=	shape function of the fluctuation amplitude
r	=	radial coordinate
St	=	Strouhal number
T	=	temperature
t	=	time
U_j	=	jet exit velocity
u_r	=	radial velocity
u_x	=	axial velocity
u_θ	=	azimuthal velocity
W	=	Chebyshev quadrature weights
W'	=	diagonal weight matrix
x	=	axial coordinate
β	=	normalized projection coefficient
γ	=	heat capacity ratio
θ	=	azimuthal coordinate
λ	=	spectral proper orthogonal decomposition eigenvalue
ρ	=	density
ϕ	=	polar coordinate
ψ_j	=	basis functions of $\boldsymbol{q}'$
ω	=	angular frequency of the fluctuations

Subscripts

f	=	end of analyzed domain
0	=	nozzle exit

Superscript

H	=	Hermitian transpose

Presented as Paper 2018-2978 at the 2018 AIAA/CEAS Aeroacoustics Conference, Atlanta, GA, June 25–29, 2018; received 18 March 2020; revision received 18 August 2020; accepted for publication 19 October 2020; published online 8 December 2020.

*luigialbieri@gmail.com.
†Assistant Professor, Aeronautic Engineering Division; andre@ita.br.
‡Assistant Professor, Department of Mechanical and Aerospace Engineering; oschmidt@ucsd.edu.
§Professor, Department of Mechanical and Civil Engineering; colonius@caltech.edu.
¶Professor, Thermal Fluids and Combustion Department, Pprime Institute; peter.jordan@univ-poitiers.fr.
**Assistant Professor, Department of Mechanical Engineering; towne@umich.edu.
††Director of Operations, Aeroacoustics; gbres@cascadetechnologies.com.

I. Introduction

JET noise remains a challenging problem in the aerospace community due to increasingly stringent noise-emission regulations.

Historically, it was thought that the main source of sound in jet flows was related to small eddies (Laurence [1]) associated with turbulence; but, more recently, large-scale structures have been shown to be a dominant source of sound. These structures initially grow exponentially through the Kelvin–Helmholtz mechanism, reach a peak, and then decay downstream, forming a wave packet. Wave packets have been observed and studied extensively; further information can be found in the works of Jordan and Colonius [2] and Cavalieri et al. [3] for linear studies and Wu an Huerre [4], Sandham and Salgado [5], and Zhang and Wu [6] for non-linear studies.

Wave-packet models have been developed to predict the behavior of large-scale turbulent structures in jets and their associated noise. The parabolized stability equations (PSEs), described by Herbert [7] and Malik et al. [8], were initially used to describe laminar–turbulent transition in slowly diverging flows. But, as shown by Gudmundsson and Colonius [9] and Sasaki et al. [10], PSEs can be used to model coherent structures in turbulent jets, especially in the near-nozzle region characterized by amplitude growth. Central in such comparisons is spectral proper orthogonal decomposition (SPOD) of flow fluctuations, as described by Picard and Delville [11] and Lumley [12]. As recently shown by Towne et al. [13], the leading SPOD mode is expected to match the optimal flow response when white-noise forcing is considered; and this optimal response can be obtained using PSEs for flows with strong convective amplification, as first pointed out by Jeun et al. [14]. This provides a basis to understand why PSE results compare favorably with the leading SPOD mode of jets.

The linear PSE has solutions with free amplitudes, which must be scaled with results from experiments or numerical simulations. This can be done in an ad hoc manner using a limited number of available measurements or in a more theoretically consistent manner by obtaining the amplitude of the Kelvin–Helmholtz mode near the nozzle exit by a projection using the adjoint mode (Rodríguez et al. [15]). Each combination of Strouhal number St and azimuthal mode m leads to a free amplitude. How such amplitudes scale with the Strouhal number St and m remains an open question. If one wishes to predict spectra of flow fluctuations using the aforementioned linear models, the frequency dependence of the amplitude is important. For lack of available information, Tam and Chen [16] assumed that wave packets are excited by white noise in time and space. Similar hypotheses have been applied in linearized models used to model wall-bounded turbulence, but it is now known that the use of "colored" excitation improves the agreement with reference data (Jovanovic and Bamieh [17], Chevalier et al. [18], and Zare et al. [19]).

In the present study, we explore how initial wave-packet amplitudes change as a function of Strouhal number and azimuthal wave number. Empirical scaling laws of wave-packet amplitude are extracted from large-eddy simulation (LES) data, allowing us to infer how they may have been excited in the flow; possible candidates involve disturbances within the nozzle boundary layer (Kaplan et al. [20]) and/or nonlinear interactions with other turbulent structures (Towne et al. [13]). The present analysis is intended to help to clarify the mechanisms underpinning the excitation of Kelvin–Helmholtz wave packets.

To derive empirical scaling laws, we will use data from the large-eddy simulations of Brès et al. [21,22]. Because the LES provides full flow information, it is suitable for detailed comparisons with PSE results. Here, we identify the free amplitude of the PSE results by minimizing the difference between the leading SPOD mode from the LES and the PSE solutions using a scalar amplitude variable. This allows us to explore how the free amplitude of the PSE wave packets change with Strouhal number St, m, and Mach number, providing insight on the mechanisms by which wave packets are excited. With a better understanding of wave-packet amplitudes, we believe scaling wave-packets, as done by source models (Wong et al. [23], Papamoschou [24], and Maia et al. [25]), can be done without the need of detailed experiments or simulation.

This paper is organized as follows. In Sec. II, we present the LES results and the PSE model, and we describe how the free amplitude of PSE solutions can be found using the leading SPOD mode from LES data. In Sec. III, we show some validation results for PSEs; then, we proceed with the determination of the wave-packet amplitudes as a function of the Strouhal number St and m, and we compare the spectrum using the identified amplitude function with LES and experimental results. The paper is completed with conclusions in Sec. IV.

II. Methods

A. Large-Eddy Simulation Database

This work relied on the numerical simulations described by Brès et al. [21] and Brès and Lele [26]. These are large-eddy simulations of isothermal subsonic jets, which exhaust from a converging-straight round nozzle, shown in Fig. 1. The boundary layer inside the nozzle is already turbulent; this was accomplished by synthetic turbulence injected at the position where a boundary-layer trip was used in accompanying experiments. For the turbulent boundary layer, a wall model was used, as described by Brès et al. [27].

Simulations were performed for Mach numbers of $M = (U_j/c_0) = 0.4$ and 0.9, based on jet exit velocity U_j and ambient sound speed c_0. A range of Mach numbers 0.4, 0.7, 0.8, and 0.9 was simulated and validated against experimental measurements [21,26]. Here, the focus is on the Mach 0.4 and 0.9 cases as representative of low- and high-subsonic jets. The corresponding Reynolds numbers are $4 \cdot 10^5$ and 10^6, respectively, using the jet diameter D as the reference length; the reference density and temperature are taken at the nozzle exit. The coordinate system used throughout this work is the same as was used in Ref. [21] and is shown in Fig. 1, where x, r, θ, and ϕ are the axial, radial, azimuthal, and polar coordinates, respectively, and the origin is at the center of the nozzle exit. All LES results are in close agreement with accompanying experiments, which were conducted at the Pprime Institute [21,26,28]. The measured turbulent flow spectra are broadbanded, and the LES results are in close agreement with experimental spectra up to a Strouhal number of 2.7.

B. Spectral Proper Orthogonal Decomposition

To isolate the dominant wave packets at each frequency and azimuthal wave number, spectral proper orthogonal decomposition was applied to the LES data. This procedure is explained in detail by Towne et al. [13]. For the round jets considered in this paper, SPOD decomposes the flow fluctuations into spatial modes that are functions of x and r for each azimuthal wave number m and Strouhal number St, i.e.,

$$\hat{\boldsymbol{q}}_{\text{spod}}(x, r, m, St) = \sum_{j=1}^{\infty} a_j(m, St)\psi_j(x, r, m, St) \tag{1}$$

The SPOD procedure expands the Fourier-transformed fluctuations $\hat{\boldsymbol{q}}_{\text{spod}}$ into orthogonal modes that optimally capture the flow energy. In Eq. (1), ψ_j are the basis functions of $\hat{\boldsymbol{q}}_{\text{spod}}$ and a_j is the amplitude captured by the mode j. The total energy is recovered by the sum over $|a_j|^2$. For this work, only the first SPOD mode at each Strouhal number St, m pair is considered because it represents the leading wave-packet properties (Schmidt et al. [29]). The SPOD modes used here are those computed by Schmidt et al. [29].

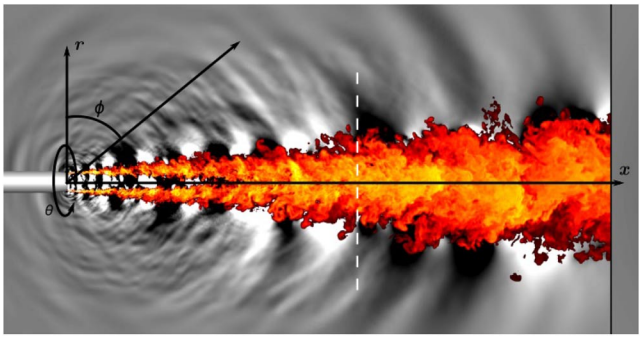

Fig. 1 Jet LES simulation with coordinate system used throughout this work.

C. Parabolized Stability Equations

1. Basic Equations

The SPOD modes taken from the large-eddy simulation do not directly provide the amplitude of the Kelvin–Helmholtz wave packets because they also comprise other flow structures. For that matter, the Kelvin–Helmholtz component needs to be derived, and this is accomplished using the parabolized stability equations. The procedure is described in what follows.

The parabolized stability equations are used to predict the fluctuation fields of the jet, using the mean turbulent field as a base flow. The PSE was first developed by Bertolotti et al. [30]; unlike the traditional Orr–Sommerfeld equation, it can be used to study the linear stability of nonparallel flows with slow divergence in the streamwise direction, including jets. The PSE procedure was traditionally used for transitional flows but, as shown in various works (Gudmundsson and Colonius [9], Cavalieri et al. [31], and Sasaki et al. [10]), it is also suitable for modeling large-scale structures in turbulent flows.

Considering flow variables written as $\boldsymbol{q}(x, r, \theta, t)$, it is possible to define a decomposition into an axisymmetric time-averaged component $\bar{\boldsymbol{q}}(x, r)$, which is used as the base flow, and a temporal fluctuation component $\boldsymbol{q}'(x, r, \theta, t)$:

$$\boldsymbol{q}(x, r, \theta, t) = \bar{\boldsymbol{q}}(x, r) + \boldsymbol{q}'(x, r, \theta, t) \tag{2}$$

The vector $\boldsymbol{q}$ refers to the flow variables $\boldsymbol{q} = (u_x, u_r, u_\theta, T, \rho)^T$, where u_x is the axial velocity, u_r is the radial velocity, u_θ is the azimuthal velocity, T is the the temperature, and ρ is the density, all in cylindrical coordinates. The jet is nonswirling, and so the mean azimuthal velocity component $\bar{u}_\theta$ is zero. The temporal fluctuation can be written as a Fourier decomposition in θ and t, shown in Eq. (3):

$$\boldsymbol{q}'(x, r, \theta, t) = \sum_{\omega} \sum_{m} \hat{\boldsymbol{q}}_{\text{pse}}(x, r, m, St) e^{im\theta} e^{-i\omega t} \tag{3}$$

In the works of Gaster [32] and Crighton and Gaster [33] an appropriate ansatz for the fluctuations Fourier decomposition $\hat{\boldsymbol{q}}_{\text{pse}}$ is derived:

$$\hat{\boldsymbol{q}}_{\text{pse}}(x, r, m, St) = \tilde{\boldsymbol{q}}(x, r, m, St) e^{i \int_{x_0}^{x_f} \alpha(\xi)\, \mathrm{d}\xi} \tag{4}$$

In Eq. (4), the term $\alpha(\xi)$ is a complex-valued hydrodynamic wave number that varies with axial direction; its imaginary part is related to exponential growth or decay of fluctuations. Also, m is the azimuthal wave number, and ω is the angular frequency of the fluctuations. In this ansatz, $\tilde{q}(x, r, m, St)$ is the shape function, which varies slowly in the streamwise direction; and the exponential term captures the fast variation related to exponential and oscillatory behavior of the large-scale turbulent structures. The combination of these two parts generates fluctuations in the shape of a wave packet.

To obtain the values of $\alpha(\xi)$ and $\tilde{\boldsymbol{q}}(x, r, m, St)$, the ansatz from Eq. (4) is substituted into a matrix system with the linearized compressible equations of continuity, momentum, and energy, resulting in a system that can be cast in matrix form as

$$[A_M(\bar{\boldsymbol{q}}, \alpha, \omega, m) + B_M(\bar{\boldsymbol{q}})]\tilde{\boldsymbol{q}} + C_M(\bar{\boldsymbol{q}}) \frac{\partial \tilde{\boldsymbol{q}}}{\partial x} + D_M(\bar{\boldsymbol{q}}) \frac{\partial \tilde{\boldsymbol{q}}}{\partial r} = 0 \tag{5}$$

Viscous terms were not considered due to the high Reynolds number of the jets considered. Details of the equation system can be found in the works of Gudmundsson and Colonius [9] and Gudmundsson [34]. The PSE code used to generate the results is described in the work of Sasaki et al. [10]. The initial fluctuation profile, in the nozzle exit plane, is given by linear stability theory, where the Kelvin–Helmholtz instability mode is found and then marched downstream by the PSE. Note that other types of waves coexisting at the same frequency and azimuthal wave number (e.g., acoustic waves or disturbances growing through the Orr mechanism [35,36]) are not captured by PSEs [37,38], leading to a wave packet dominated by the Kelvin–Helmholtz mode. For this case, the base flow used is a time-averaged mean flow taken from the large-eddy simulation, which was described in the previous section.

The domain was discretized numerically using 301 Chebyshev nodes in the r direction, as well as by using the mapping function from Lesshafft and Huerre [39] to concentrate points in the jet region. The solution is advanced in the downstream x direction using an implicit Euler method.

We are interested in determining the behavior of wave-packet amplitudes as a function of the Strouhal number St and m. To define these amplitudes in a consistent manner, the linear PSE solutions must be normalized in a definite way. We have adopted, as the normalization condition, that flow fluctuations at the nozzle exit ($x = 0$) have unit norm. This is ensured by rescaling $\tilde{\boldsymbol{q}}_0 = \tilde{\boldsymbol{q}}(x = 0, r, m, St)$ such that

$$\tilde{\boldsymbol{q}}_0^H W' \tilde{\boldsymbol{q}}_0 = 1 \tag{6}$$

with W' as a diagonal weight matrix given by

$$W' = \text{diag} \quad W\bar{\rho}_0, W\bar{\rho}_0, W\bar{\rho}_0, W\frac{\bar{T}_0}{\gamma \bar{\rho}_0 M^2}, W\frac{\bar{\rho}_0}{\gamma(\gamma - 1)\bar{T}_0 M^2} \Bigg) \tag{7}$$

where the superscript H denotes the Hermitian transpose, and the subscript 0 denotes properties at the nozzle exit. The matrix W contains Chebyshev quadrature weights for integration over the radius. The inner product defined with W' corresponds to the Chu norm used by Schmidt et al. [29]. The present definition thus normalizes the PSE solution such that the initial Kelvin–Helmholtz mode, taken at $x = 0$, has unit norm.

2. Study of Wave-Packet Amplitudes Using PSE and SPOD Modes

The normalization described in the previous section leads to an amplitude for the PSE solution that may not be representative of flow fluctuations for the given Strouhal number St and m; the PSE solutions require rescaling using simulation data. The values in the near-nozzle region of the jet were used to calculate a scaling factor between PSE results and the first SPOD mode educed from the LES data. This scaling factor A is used to adjust the free amplitude of the linear PSE solutions so as to minimize the difference E given by

$$E = \left\| \sqrt{\lambda}\hat{\boldsymbol{q}}_{\text{spod}} - A\hat{\boldsymbol{q}}_{\text{pse}} \right\| \tag{8}$$

where λ is the SPOD eigenvalue whose value is equal to the power spectral density (energy) of flow fluctuations for the corresponding SPOD eigenfunction. Rescaling the orthonormal SPOD modes by $\sqrt{\lambda}$ leads to amplitudes that are representative of the mode contribution to the full LES fields, as shown by Sinha et al. [40].

A is a complex-valued scalar value, and its optimal value is obtained by minimizing the error E separately at each m and Strouhal number St combination. Setting the derivative of E with respect to the amplitude A to zero leads to

$$\left\langle \sqrt{\lambda}\hat{\boldsymbol{q}}_{\text{spod}}, \hat{\boldsymbol{q}}_{\text{pse}} \right\rangle - A\left\langle \hat{\boldsymbol{q}}_{\text{pse}}, \hat{\boldsymbol{q}}_{\text{pse}} \right\rangle = 0$$

and thus the optimal amplitude is

$$A = \frac{\left\langle \sqrt{\lambda}\hat{\boldsymbol{q}}_{\text{spod}}, \hat{\boldsymbol{q}}_{\text{pse}} \right\rangle}{\left\langle \hat{\boldsymbol{q}}_{\text{pse}}, \hat{\boldsymbol{q}}_{\text{pse}} \right\rangle} \tag{9}$$

The inner product in Eq. (9) induces the norm in Eq. (8), and thus defines the sense in which the error is minimized. Since $\hat{\boldsymbol{q}}_{\text{spod}}$ and $\hat{\boldsymbol{q}}_{\text{pse}}$

are functions of x and r, and depend parametrically on Strouhal number St and m, we define the inner product as

$$\langle f(r,x,St,m), g(r,x,St,m)\rangle = \int_{x_o}^{x_f}\int_0^{\infty}(f(x,r,St,m)g^*(x,r,St,m))r\,\mathrm{d}r\,\mathrm{d}x \qquad (10)$$

and consider only the pressure component in $\hat{\boldsymbol{q}}_{\mathrm{spod}}$ and $\hat{\boldsymbol{q}}_{\mathrm{pse}}$. This is due to a smoother behavior of $A(St)$ observed when pressure is taken as the relevant flow quantity. However, considering velocity fluctuations or the full disturbance vector leads to similar results. Since azimuthal modes are orthogonal to each other, no azimuthal integration is required. This leads to an amplitude of $A(St, m)$, depending on the Strouhal number and azimuthal wave number. The argument of the complex-valued amplitude A in Eq. (9) also allows us to set the phase of the PSE solution for a best match with the SPOD mode. It is possible to apply this method by considering the whole domain but, as illustrated in Sec. III, the PSE has good agreement with the leading SPOD mode for a limited axial range for each Strouhal number St. Thus, limiting the domain will lead to more precise results. The trapezoid rule is used to calculate the integral in the inner product. The PSE uses a different grid from the LES results, and therefore an interpolation was required to obtain values for the same x.

Unlike global stability modes, the linear PSE does not provide a basis for flow fluctuations; PSE results are the solution of a boundary-value problem, with nonzero boundary conditions at the nozzle exit, and not eigenfunctions of a linear operator. Hence, strictly speaking, one cannot think of the aforementioned procedure as a projection, as is often done for stability eigenfunctions (Rodríguez et al. [15,41]). However, here, we are interested in the determination of the amplitude of a single spatial function, and thus the approach can be used as a method to estimate wave-packet amplitudes by considering a jet region between x_o and x_f.

III. Results

A. Showing the PSE Results

The first step is to obtain PSE wave packets and validate them by comparison with the first SPOD modes educed from the LES data. The PSE code was run for Mach numbers of 0.4 and 0.9, as well as for Strouhal numbers St varying from 0.0488 to 1.6113 for the $M = 0.4$ case and from 0.0868 to 2.778 for the $M = 0.9$ case. These Strouhal number ranges were chosen due to the range of expected agreement between the PSE and the SPOD data [9,10] so as to capture the exponential behavior with less influence from fluctuations other than the Kelvin–Helmholtz wave packet that show up in very low and high Strouhal numbers St. We thus focus on the parameter range with dominance of linear behavior, justifying the neglect of nonlinear terms in PSEs.

The Strouhal numbers used are those of the SPOD results to facilitate comparison. The first three azimuthal modes are calculated ($m = 0, 1, 2$). A comparison of pressure fluctuations is shown for two representative Strouhal numbers St, and it is restricted to the axisymmetric mode of $m = 0$ for brevity. The Strouhal numbers are $St = 0.44$ and 1.22 for $M = 0.4$, and $St = 0.61$ and 1.39 for $M = 0.9$. The amplitude and phase of the PSE solution were adjusted using Eq. (9). These results are shown in Fig. 2.

It is possible to see a close agreement between the PSE and the first SPOD modes for a good range of frequencies, especially in the upstream region, characterized by amplitude growth associated with the Kelvin–Helmholtz mechanism. For downstream points, there is a growing mismatch, which was explored by Tissot et al. [36]. The present code was previously used by Sasaki et al. [42] and showed agreement for an LES data Strouhal number as high as four.

B. Amplitude Scaling

The results from Sasaki et al. [42] are used to select appropriate integration limits in the definition of the inner product [Eq. (10)], which define the regions where the PSE solutions and SPOD modes

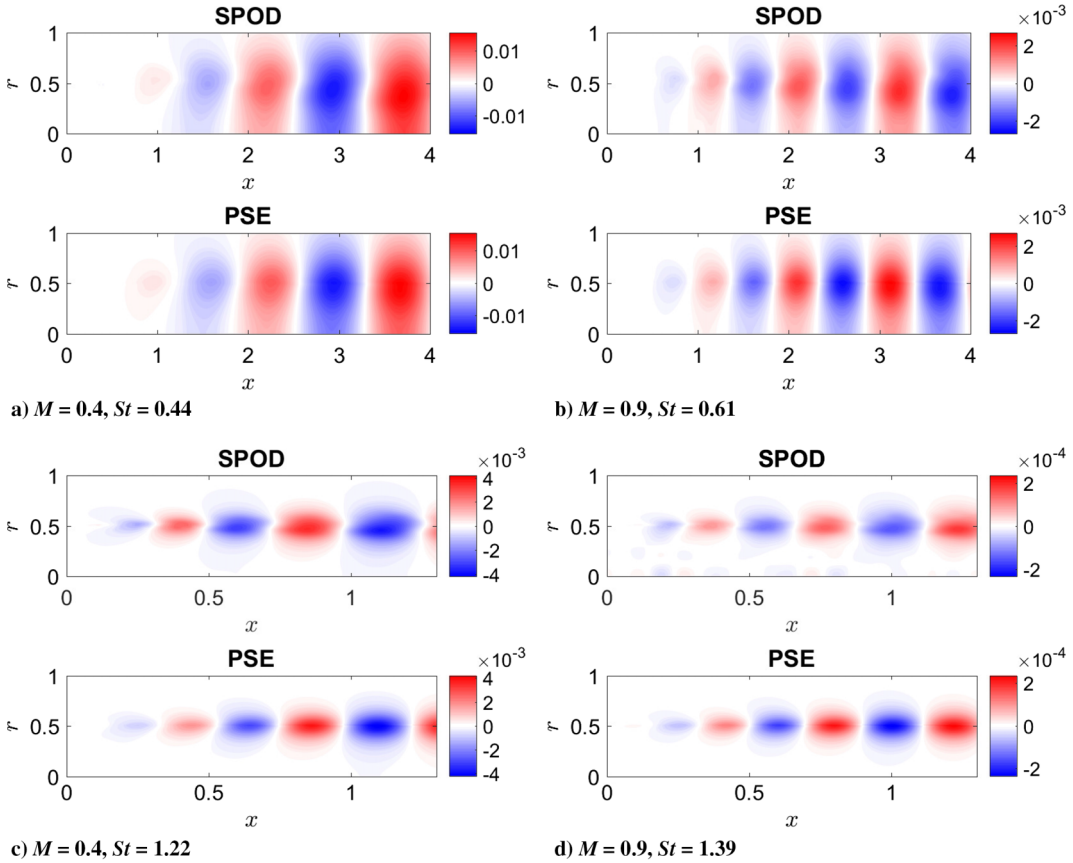

Fig. 2 Pressure fluctuation contour for azimuthal mode $m = 0$ for Mach numbers 0.4 and 0.9, for two sample Strouhal numbers St each.

are compared to determine the desired amplitudes. Sasaki et al. [42] showed a normalized projection coefficient β between SPOD and PSE results at each x station of the jet. The expression for β is

$$\beta(x, St, m) = \frac{|\langle \boldsymbol{q}'_{\text{spod}}(x, r, St, m), \boldsymbol{q}'_{\text{pse}}(x, r, St, m)\rangle|}{\|\boldsymbol{q}'_{\text{spod}}(x, r, St, m)\| \|\boldsymbol{q}'_{\text{pse}}(x, r, St, m)\|} \tag{11}$$

where the inner product considers only radial integration in Eq. (10) so as to indicate a local level of agreement at a station x. $\beta = 1$ is in perfect agreement, and $\beta = 0$ is obtained when the PSE result at a given station x is orthogonal to the corresponding SPOD result. Such an agreement metric is shown in Fig. 3 for $M = 0.4$ and in Fig. 4 for $M = 0.9$.

To ensure that the amplitude scaling is trustworthy, the region of the jet flow used is delimited by the yellow rectangles in Figs. 3 and 4; these upstream regions correspond to exponential growth of wave packets associated with the Kelvin–Helmholtz mechanism [41], as well as with good agreement between PSEs and experimental or numerical results (Gudmundsson and Colonius [9], Cavalieri et al. [31], Tissot et al. [36], Sasaki et al. [42]). Therefore, the ranges of the scaling will be $x/D \in [x_o = 0.5, x_f = 1.5]$, $St \in [0, 1.6]$ for $M = 0.4$, and $St \in [0, 2.5]$ for $M = 0.9$. The amplitude identification was performed for $M = 0.4$ and 0.9, as well as the first three azimuthal modes of $m = 0, 1, 2$. These lower azimuthal wave numbers are known to dominate the peak of far-field spectra [21,43]. As commented earlier, the pressure fluctuations were used to obtain the amplitudes.

The absolute value of the amplitudes calculated using this choice of inner product are shown in Fig. 5 for $M = 0.4$ and $M = 0.9$. Even though observable oscillations are present in these plots, there is clearly an exponential decay of the absolute value of the amplitude with the increasing of the Strouhal number St. An exponential fit was applied to the data, yielding a function $|A|(St)$ that may be used to scale the wave-packet models. The fitting function is given by

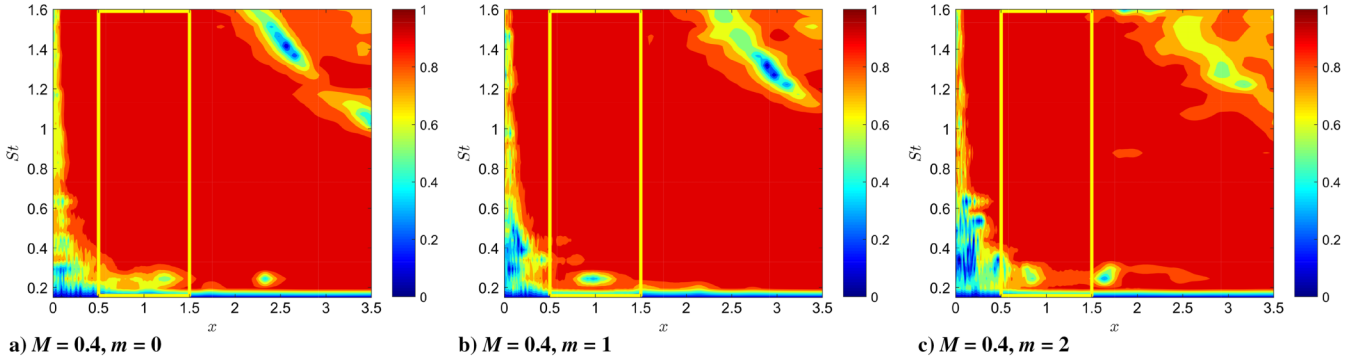

a) $M = 0.4, m = 0$ b) $M = 0.4, m = 1$ c) $M = 0.4, m = 2$

Fig. 3 Metric for agreement between SPOD mode and PSE for $m = 0, 1, 2$ for $M = 0.4$; yellow rectangles indicate the regions used for amplitude scaling in the present work.

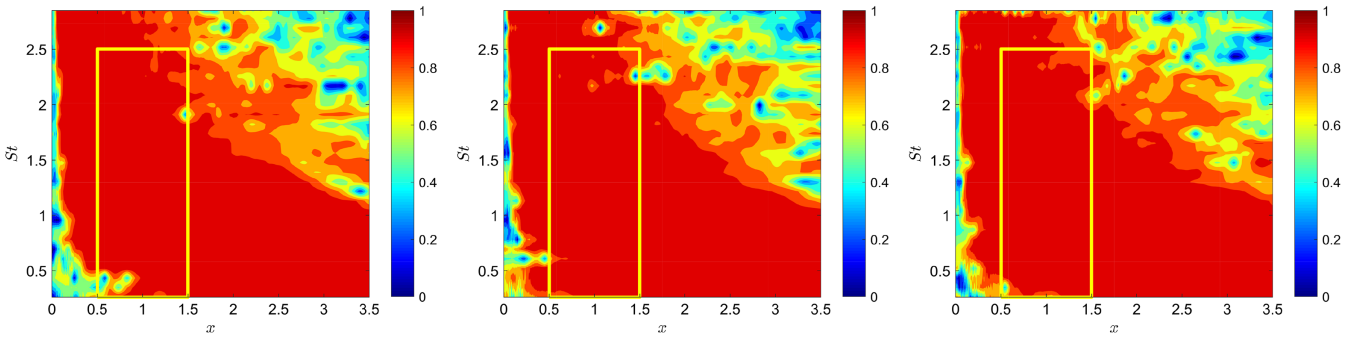

a) $M = 0.9, m = 0$ b) $M = 0.9, m = 1$ c) $M = 0.9, m = 2$

Fig. 4 Metric for agreement between SPOD mode and PSE for $m = 0, 1, 2$ for $M = 0.9$; yellow rectangles indicate the regions used for amplitude scaling in the present work.

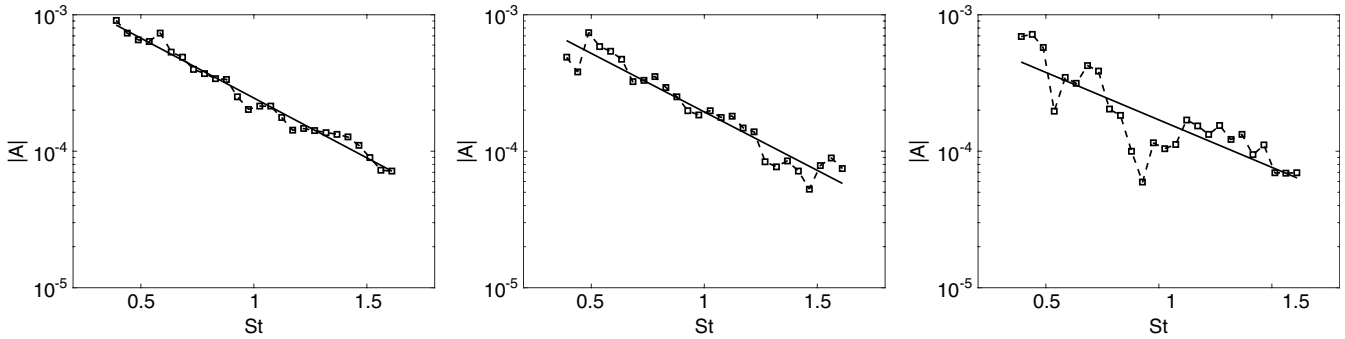

a) $M = 0.4, m = 0$ b) $M = 0.4, m = 1$ c) $M = 0.4, m = 2$

Fig. 5 Curve fit for scaling factor, in semilog scale, for $M = 0.4$: dashed lines denote original scaling factor obtained by Eq. (9) with (squares) data points, and solid lines denote exponential fit of the black curve, with values shown in Table 1.

Table 1 Fit obtained from amplitude in function of Strouhal number St, where C and κ are the coefficients of the exponential equation $|A|(St) = Ce^{\kappa St}$

M	m	C	κ
0.4	0	$1.85 \cdot 10^{-3}$	−2.02
0.4	1	$1.40 \cdot 10^{-3}$	−1.97
0.4	2	$8.42 \cdot 10^{-4}$	−1.60
0.9	0	$6.34 \cdot 10^{-4}$	−3.01
0.9	1	$5.10 \cdot 10^{-4}$	−3.05
0.9	2	$2.07 \cdot 10^{-4}$	−2.52

$$|A|(St) = Ce^{\kappa St} \tag{12}$$

with C and κ coefficients reported in Table 1. The exponential fits are shown in Figs. 5 and 6, which refer to $M = 0.4$ and 0.9, respectively. An accurate representation of the amplitude behavior is obtained with the fitting functions. However, the azimuthal mode of $m = 2$ for the Mach 0.4 jet has more marked oscillations whose origins are unclear at this time. However, even in the latter case, the general trend of amplitude decay with increasing Strouhal number St is retrieved with coefficients that are similar to the other cases.

Only the absolute value of A is relevant, since the phase in a specific point is arbitrary due to the stochastic nature of the jet. The leading SPOD modes are eigenfunctions, and thus have an arbitrary phase for each frequency; such a phase is retrieved in the argument of A and allows a visual comparison such as in Fig. 2, but the precise value of phase is not of particular interest.

C. Modeled Spectra

The Strouhal number dependencies obtained in the previous section can be used to estimate power spectra at given positions of the flow; an accurate representation of spectra is a useful consistency check and shows whether the proposed exponential fits, once taken as initial PSE amplitudes, may accurately describe flow fluctuations for a range of Strouhal numbers St. Pressure spectra on the jet lip line and centerline were chosen to plot and compare the spectra between the PSE model and the LES. These spectra are representative of near-field disturbances within the jet. Results are shown in Figs. 7–10. Figures 7 and 8 display centerline comparisons for $M = 0.4$ and 0.9, respectively. Corresponding lip-line spectra are shown in Figs. 9 and 10. Centerline comparisons are restricted to $m = 0$ because this is the sole azimuthal wave number with nonzero amplitude on the jet axis. Spectra on the lip line are shown for $m = 0$, 1, and 2.

There is an overall good agreement between PSE results scaled with the amplitude fits in Table 1 and the pressure spectra, except for low Strouhal numbers, at which a mismatch between PSE and turbulent jet data can be associated with mechanisms other than Kelvin–Helmholtz (Schmidt et al. [29] and Lesshafft and Huerre [39]). For $St < 0.2$, some discontinuity appears, in view of the fact that the domain is not large enough.

For higher Strouhal numbers St, there is also a mismatch, possibly due to flow structures other than Kelvin–Helmholtz wave packets with significant contributions at the considered positions. For the Mach 0.9 jet, oscillations in the spectra near the nozzle are observed; these are related to trapped acoustic waves (Towne et al. [44] and Schmidt et al. [45]), which are not modeled in the PSE solution; however, the downstream spectra are dominated by the Kelvin–Helmholtz contribution, and thus accurately represented by PSEs, with the amplitudes in Table 1.

Our results were obtained by solely considering pressure fluctuations in determination of the amplitude described in Sec. II.C.2. The same approach was also applied by considering the streamwise velocity u_x, and similar results were obtained. Similar trends can be seen in the comparison between the velocity spectrum of the scaled PSE and the experimental results by Cavalieri et al. [31],

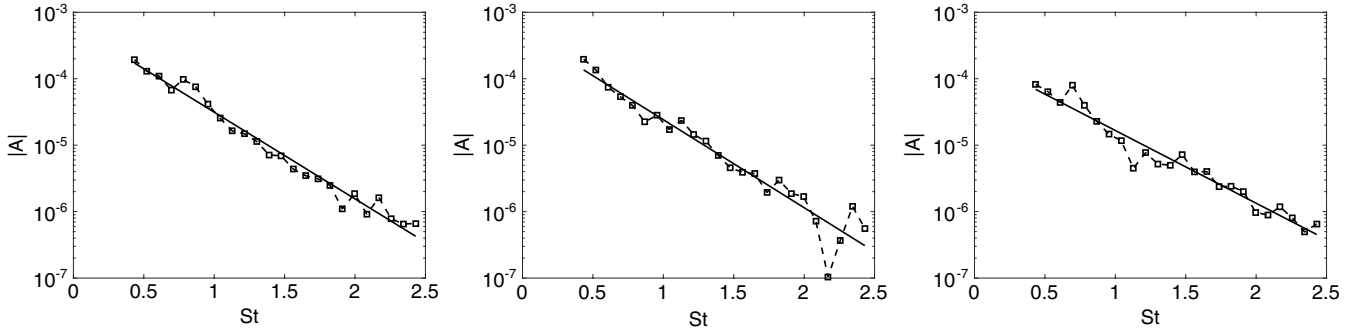

Fig. 6 Curve fit for scaling factor, in semilog scale, for $M = 0.9$: dashed lines denote original scaling factor obtained by Eq. (9) with (squares) data points, and solid lines denote exponential fit of the black curve, with values shown in Table 1.

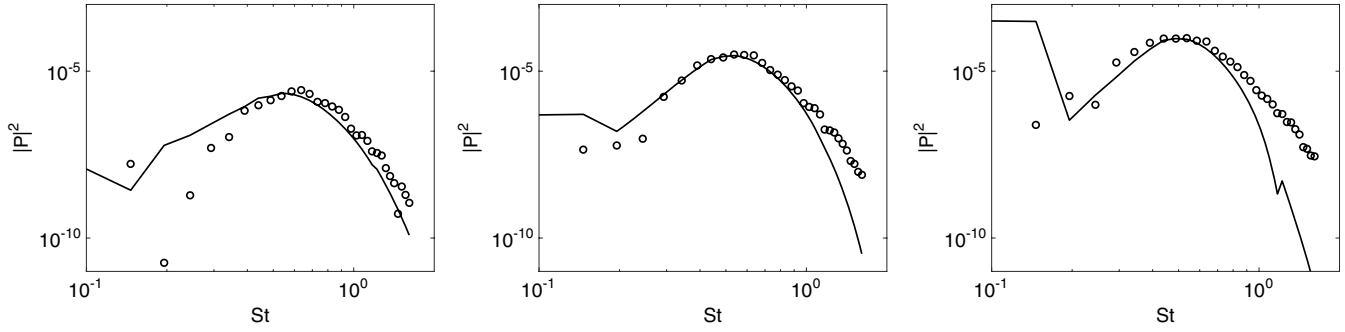

Fig. 7 Centerline ($r/D = 0$) spectrum using scaling factor of pressure fluctuations for $M = 0.4$ case, for $m = 0$ and $x/D = 1$, 2, 3: PSE results (solid lines), and LES values (circles).

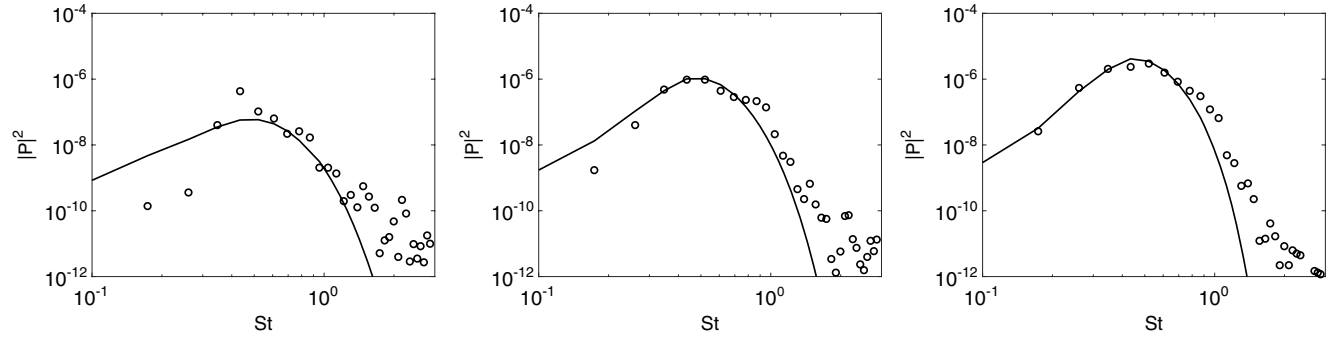

a) $M = 0.9$, $m = 0$, $x/D = 1$ **b) $M = 0.9$, $m = 0$, $x/D = 2$** **c) $M = 0.9$, $m = 0$, $x/D = 3$**

Fig. 8 Centerline ($r/D = 0$) spectrum using scaling factor of pressure fluctuations for $M = 0.9$ case, for $m = 0$ and $x/D = 1, 2, 3$: PSE results (solid lines), and LES values (circles).

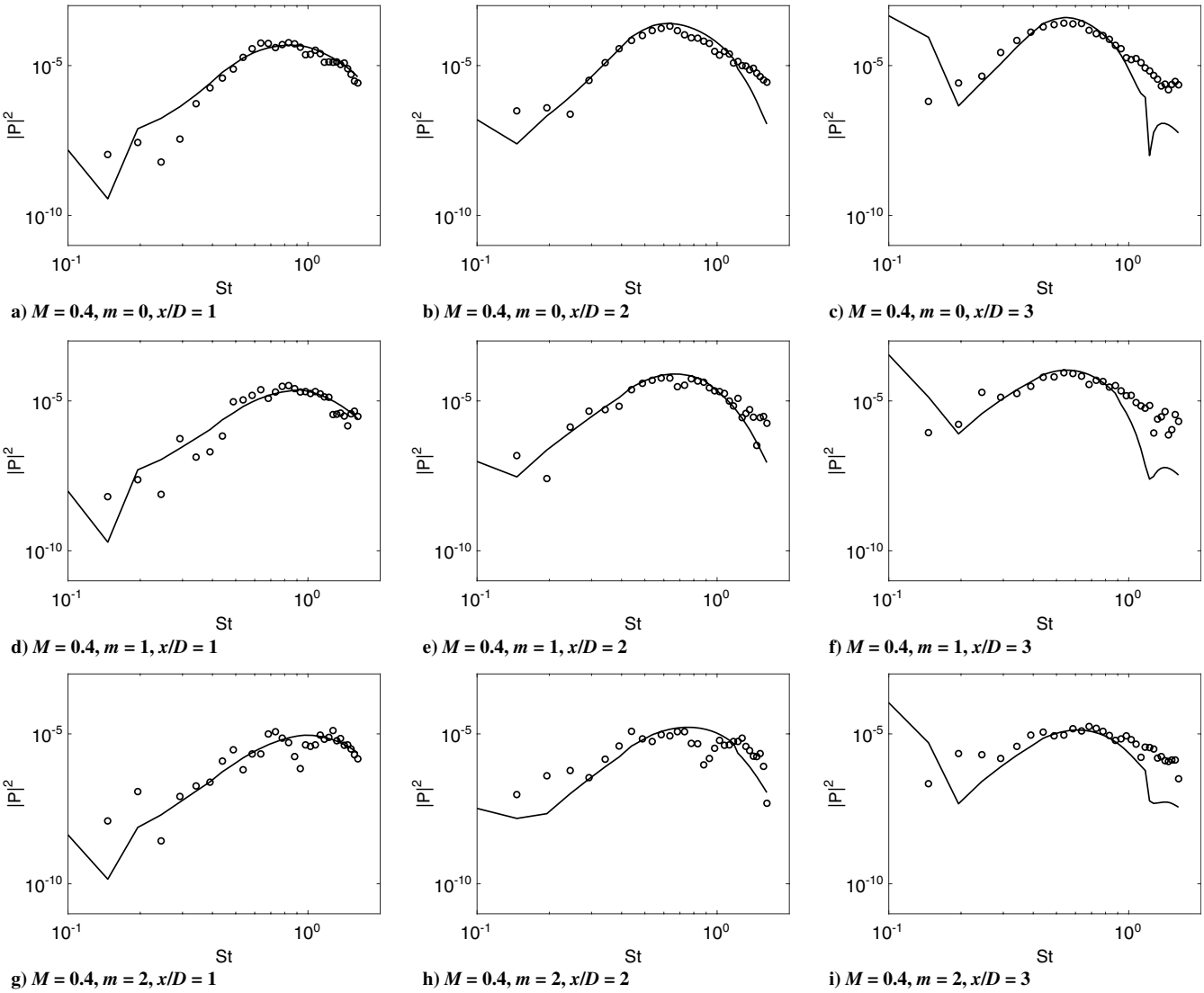

a) $M = 0.4$, $m = 0$, $x/D = 1$ **b) $M = 0.4$, $m = 0$, $x/D = 2$** **c) $M = 0.4$, $m = 0$, $x/D = 3$**

d) $M = 0.4$, $m = 1$, $x/D = 1$ **e) $M = 0.4$, $m = 1$, $x/D = 2$** **f) $M = 0.4$, $m = 1$, $x/D = 3$**

g) $M = 0.4$, $m = 2$, $x/D = 1$ **h) $M = 0.4$, $m = 2$, $x/D = 2$** **i) $M = 0.4$, $m = 2$, $x/D = 3$**

Fig. 9 Lip-line ($r/D = 0.5$) spectrum using scaling factor of pressure fluctuations for $M = 0.4$ case, for $m = 0, 1, 2$ and $x/D = 1, 2, 3$: PSE results (solid lines), and LES values (circles).

where good agreement is obtained again for the Mach 0.4 jet in Fig. 11.

The results show that the initial absolute value of the amplitude of turbulent jet wave packets has an exponential dependence on the Strouhal number St. Amplitudes change by about two orders of magnitude in the Strouhal range considered. It is thus clear that the excitation of wave packets at the nozzle exit cannot be considered as white noise, with the same amplitude for all Strouhal numbers St. This can be further appreciated if a Strouhal number St-independent amplitude is considered for PSEs; lip-line $m = 0$ spectra generated with such an assumption are shown in Figs. 12 and 13. Comparison of these figures to the amplitude-scaled results in Figs. 9 and 10

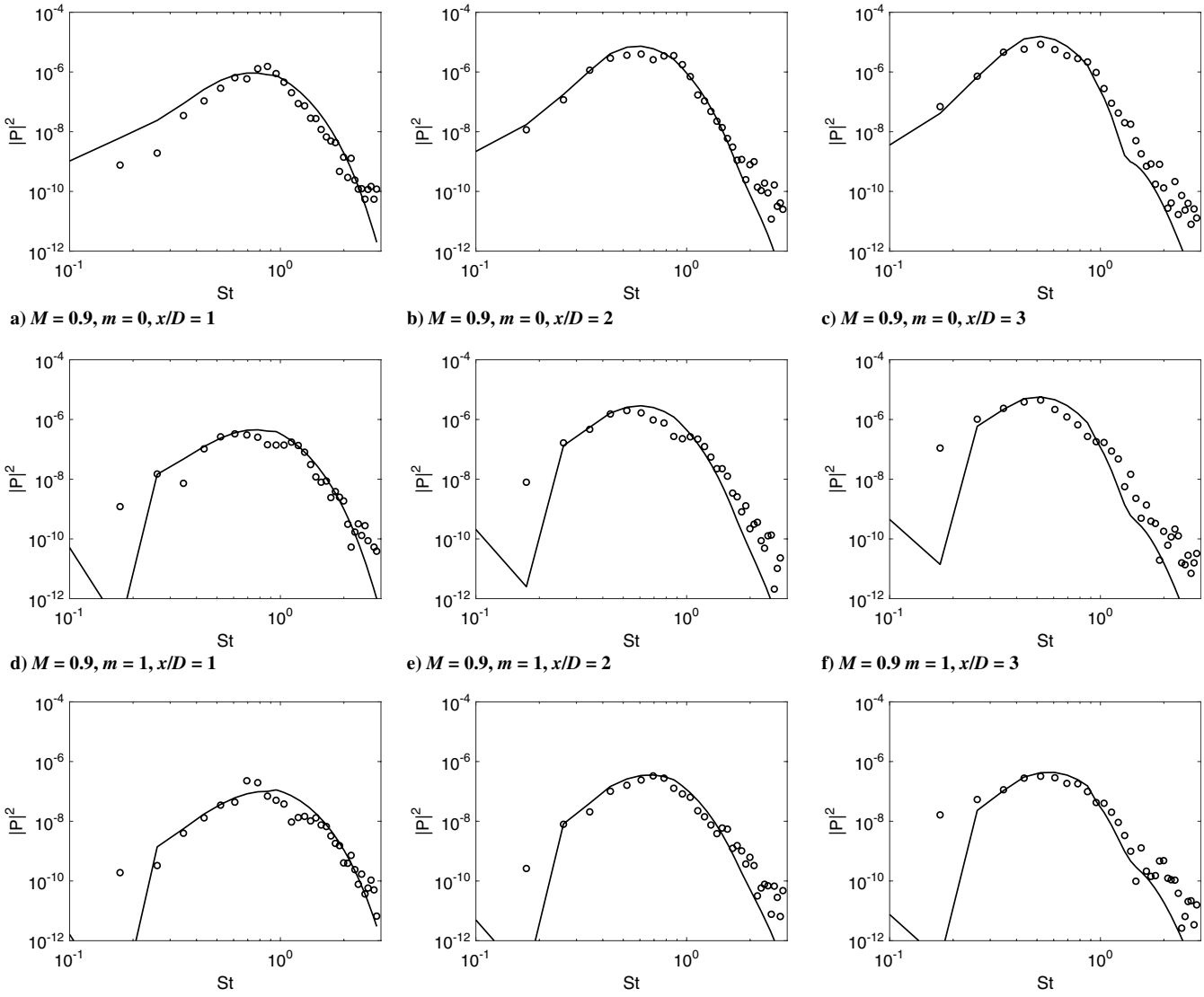

a) $M = 0.9$, $m = 0$, $x/D = 1$ **b)** $M = 0.9$, $m = 0$, $x/D = 2$ **c)** $M = 0.9$, $m = 0$, $x/D = 3$

d) $M = 0.9$, $m = 1$, $x/D = 1$ **e)** $M = 0.9$, $m = 1$, $x/D = 2$ **f)** $M = 0.9$ $m = 1$, $x/D = 3$

g) $M = 0.9$, $m = 2$, $x/D = 1$ **h)** $M = 0.9$, $m = 2$, $x/D = 2$ **i)** $M = 0.9$, $m = 2$, $x/D = 3$

Fig. 10 Lip-line ($r/D = 0.5$) spectrum using scaling factor of pressure fluctuations for the $M = 0.9$ case, for $m = 0, 1, 2$ and $x/D = 1, 2, 3$: PSE results (solid lines), and LES values (circles).

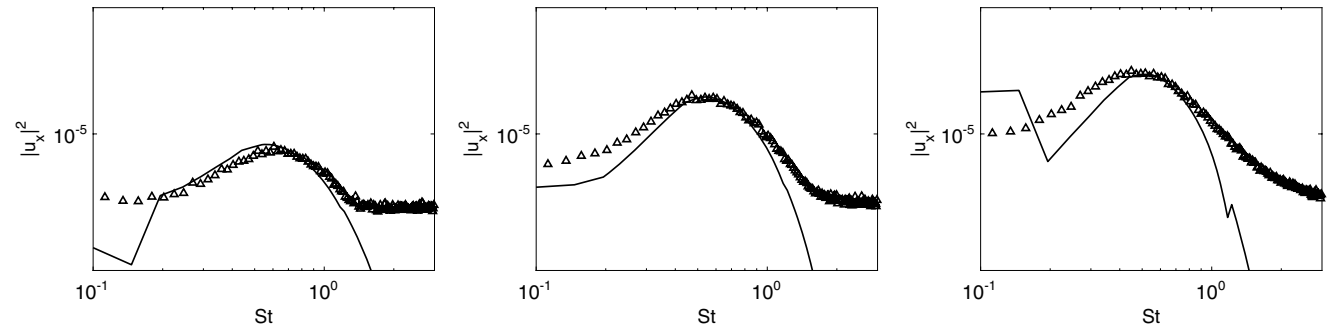

a) $M = 0.4$, $m = 0$, $x/D = 1$ **b)** $M = 0.4$, $m = 0$, $x/D = 2$ **c)** $M = 0.4$, $m = 0$, $x/D = 3$

Fig. 11 Centerline ($r/D = 0$) spectrum using the scaling factor of axial velocity fluctuations for the $M = 0.4$ case, for $m = 0$ and $x/D = 1, 2, 3$: PSE results (solid lines), and experimental data (triangles) [31].

highlights that the exponential decay of amplitude with increasing Strouhal number St is an important dynamic feature required to obtain spectral shapes accurately. Improvements on methods such as that by Tam and Chen [16] may be obtained if the observed exponential dependence in amplitude is included in models.

IV. Conclusions

The frequency dependence of turbulent jet wave-packet amplitudes is studied by an approach that consists of minimizing the difference in amplitude between linear PSE results and the leading SPOD mode educed from a well validated large-eddy simulation. This procedure,

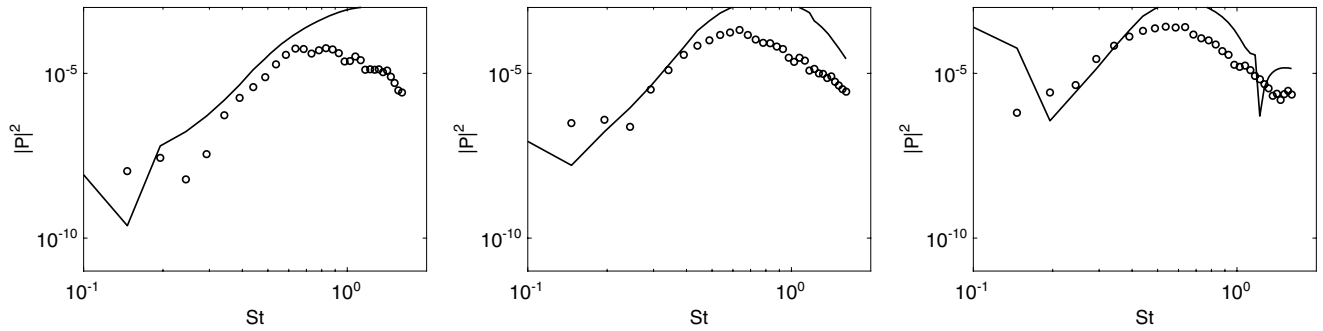

a) $M = 0.4$, $m = 0$, $x/D = 1$ **b) $M = 0.4$, $m = 0$, $x/D = 2$** **c) $M = 0.4$, $m = 0$, $x/D = 3$**

Fig. 12 Lip-line ($r/D = 0.5$) spectrum using a amplitude (white-noise forcing) taken for $St = 0.2$ results for the $M = 0.4$ case, for $m = 0$ and $x/D = 1, 2, 3$: PSE results (solid lines), and LES values (circles).

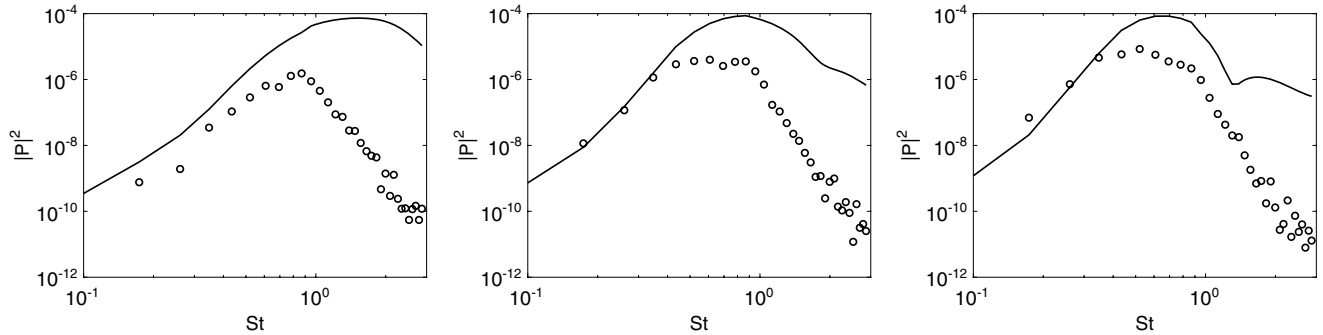

a) $M = 0.9$, $m = 0$, $x/D = 1$ **b) $M = 0.9$, $m = 0$, $x/D = 2$** **c) $M = 0.9$, $m = 0$, $x/D = 3$**

Fig. 13 Lip-line ($r/D = 0.5$) spectrum using amplitude (white-noise forcing) taken for $St = 0.2$ results for the $M = 0.9$ case, for $m = 0$ and $x/D = 1, 2, 3$: PSE results (solid lines), and LES values (circles).

which is applied for a region of the flow where linear PSE has been shown to agree with numerical and experimental data, leads to wave-packet amplitudes with an exponential dependence on Strouhal number. Exponential fits are obtained for azimuthal wave numbers of $m = 0$, 1, and 2; and for Mach numbers of $M = 0.4$ and 0.9. These fits were shown to accurately predict, in good agreement, the power spectra of the flow, matching simulation and experimental data.

The amplitude scaling results may serve as a basis to study the receptivity mechanisms of Kelvin–Helmholtz wave packets in turbulent jets. An open question regarding such wave packets is related to their excitation; the exponential dependence seen here can serve as a test of proposed mechanisms and models, which should be able to reproduce the amplitude scaling observed in the present paper. The consistency of the same kind of fit for different Mach numbers is another indication of the clear exponential scaling of the wave packets.

The next step is to understand how the wave packets with this behavior are excited. In the current case, the turbulent boundary layer inside the nozzle is a clear candidate for an excitation mechanism; this has been explored by Kaplan et al. [20] but requires further study. The determination of the physical mechanism underpinning the observed exponential decay of amplitude with increasing Strouhal number St is a future prospect of this work. The determination of amplitudes requires use of LES data, and is thus an empirical determination of Kelvin–Helmholtz wave-packet amplitudes. Nonlinear models (Wu and Huerre [4], Sandham and Salgado [5], and Zhang and Wu [6]) may directly provide such amplitudes from first principles, especially if coupled to the nozzle boundary-layer dynamics.

The present results can be used to scale wave-packet models in jets if detailed data from experiments or simulations are not available; a recent example is the work of Wong et al. [23], where wave-packet source models with a proper amplitude scaling are used in an acoustic analogy to obtain broadband-shock-associated noise from supersonic jets. The present results may be used in acoustic predictions based on other kinematic source models' jet wave packets, such as in the works of Papamoschou [24] or Maia et al. [25].

Acknowledgments

Luigi Antonialli had financial support from Coordenação de Aperfeiçoamento de Pessoal de Nível Superior (Capes) by a M.S. scholarship. This project had funding from Financiadora de Estudos e Projetos (FINEP) and Embraer through grant 137/18. The large-eddy simulation studies were supported by Naval Air Systems Command Small Business Innovation Research (NAVAIR SBIR) projects with computational resources provided by the U.S. Department of Defense's High Performance Computing Modernization Program (HPCMP). The authors acknowledge Kenzo Sasaki for providing the data and code used in this paper, as well as Instituto Tecnológico de Aeronáutica (ITA) for supporting this project with the necessary resources.

References

[1] Laurence, J. C., "Intensity, Scale, and Spectra of Turbulence in Mixing Region of Free Subsonic Jet," NACA TR-1292, 1956.

[2] Jordan, P., and Colonius, T., "Wave Packets and Turbulent Jet Noise," *Annual Review of Fluid Mechanics*, Vol. 45, Jan. 2013, pp. 173–195. https://doi.org/10.1146/annurev-fluid-011212-140756

[3] Cavalieri, A., Jordan, P., and Lesshafft, L., "Wave-Packet Models for Jet Dynamics and Sound Radiation," *Applied Mechanics Reviews*, Vol. 71, No. 2, 2019, Paper 020802. https://doi.org/10.1115/1.4042736

[4] Wu, X., and Huerre, P., "Low-Frequency Sound Radiated by a Nonlinearly Modulated Wavepacket of Helical Modes on a Subsonic Circular Jet," *Journal of Fluid Mechanics*, Vol. 637, Oct. 2009, pp. 173–211. https://doi.org/10.1017/s0022112009990577

[5] Sandham, N. D., and Salgado, A. M., "Nonlinear Interaction Model of Subsonic Jet Noise," *Philosophical Transactions of the Royal Society of London, Series A: Mathematical, Physical and Engineering Sciences*, Vol. 366, No. 1876, 2008, pp. 2745–2760. https://doi.org/10.1098/rsta.2008.0049

[6] Zhang, Z., and Wu, X., "Nonlinear Evolution and Acoustic Radiation of Coherent Structures in Subsonic Turbulent Free Shear Layers," *Journal of Fluid Mechanics*, Vol. 884, Feb. 2020, Paper A10. https://doi.org/10.1017/jfm.2019.909

[7] Herbert, T., "Parabolized Stability Equations," *Annual Review of Fluid Mechanics*, Vol. 29, No. 1, 1997, pp. 245–283. https://doi.org/10.1146/annurev.fluid.29.1.245

[8] Malik, M., Chuang, S., and Hussaini, M., "Accurate Numerical Solution of Compressible, Linear Stability Equations," *Zeitschrift für Angewandte Mathematik und Physik*, Vol. 33, No. 2, 1982, pp. 189–201. https://doi.org/10.1007/BF00944970

[9] Gudmundsson, K., and Colonius, T., "Instability Wave Models for the Near-Field Fluctuations of Turbulent Jets," *Journal of Fluid Mechanics*, Vol. 689, Dec. 2011, pp. 97–128. https://doi.org/10.1017/jfm.2011.401

[10] Sasaki, K., Piantanida, S., Cavalieri, A. V., and Jordan, P., "Real-Time Modelling of Wavepackets in Turbulent Jets," *Journal of Fluid Mechanics*, Vol. 821, June 2017, pp. 458–481. https://doi.org/10.2514/6.2015-2214

[11] Picard, C., and Delville, J., "Pressure Velocity Coupling in a Subsonic Round Jet," *International Journal of Heat and Fluid Flow*, Vol. 21, No. 3, 2000, pp. 359–364. https://doi.org/10.1016/S0142-727X(00)00021-7

[12] Lumley, J. L., *Stochastic Tools in Turbulence*, Courier Corp., Chelmsford, MA, 2007.

[13] Towne, A., Schmidt, O. T., and Colonius, T., "Spectral Proper Orthogonal Decomposition and Its Relationship to Dynamic Mode Decomposition and Resolvent Analysis," *Journal of Fluid Mechanics*, Vol. 847, July 2018, pp. 821–867.

[14] Jeun, J., Nichols, J. W., and Jovanović, M. R., "Input-Output Analysis of High-Speed Axisymmetric Isothermal Jet Noise," *Physics of Fluids*, Vol. 28, No. 4, 2016, Paper 047101. https://doi.org/10.1063/1.4946886

[15] Rodrguez, D., Sinha, A., Brès, G. A., and Colonius, T., "Inlet Conditions for Wave Packet Models in Turbulent Jets Based on Eigenmode Decomposition of Large Eddy Simulation Data," *Physics of Fluids*, Vol. 25, No. 10, 2013, Paper 105107. https://doi.org/10.1063/1.4824479

[16] Tam, C. K., and Chen, P., "Turbulent Mixing Noise from Supersonic Jets," *AIAA Journal*, Vol. 32, No. 9, 1994, pp. 1774–1780. https://doi.org/10.2514/3.12173

[17] Jovanovic, M., and Bamieh, B., "The Spatio-Temporal Impulse Response of the Linearized Navier-Stokes Equations," *Proceedings of the 2001 American Control Conference (Cat. No. 01CH37148)*, Vol. 3, Inst. of Electrical and Electronics Engineers, New York, 2001, pp. 1948–1953. https://doi.org/10.1109/ACC.2001.946026

[18] Chevalier, M., Hœpffner, J., Bewley, T. R., and Henningson, D. S., "State Estimation in Wall-Bounded Flow Systems. Part 2. Turbulent Flows," *Journal of Fluid Mechanics*, Vol. 552, No. 1, 2006, pp. 167–187. https://doi.org/10.1017/S0022112005008578

[19] Zare, A., Jovanović, M. R., and Georgiou, T. T., "Colour of Turbulence," *Journal of Fluid Mechanics*, Vol. 812, Feb. 2017, pp. 636–680. https://doi.org/10.1017/jfm.2016.682

[20] Kaplan, O., Jordan, P., and Cavalieri, A. V., "Exploring the Link Between Nozzle Dynamics and Wavepackets in a Mach 0.9 Turbulent Jet," *23rd AIAA/CEAS Aeroacoustics Conference*, AIAA Paper 2017-3708, 2017. https://doi.org/10.2514/6.2017-3708

[21] Brès, G. A., Jordan, P., Jaunet, V., Le Rallic, M., Cavalieri, A. V., Towne, A., Lele, S. K., Colonius, T., and Schmidt, O. T., "Importance of the Nozzle-Exit Boundary-Layer State in Subsonic Turbulent Jets," *Journal of Fluid Mechanics*, Vol. 851, Sept. 2018, pp. 83–124. https://doi.org/10.1017/jfm.2018.476

[22] Brès, G. A., Ham, F. E., Nichols, J. W., and Lele, S. K., "Unstructured Large-Eddy Simulations of Supersonic Jets," *AIAA Journal*, Vol. 55, No. 4, 2017, pp. 1164–1184. https://doi.org/10.2514/1.J055084

[23] Wong, M. H., Jordan, P., Honnery, D. R., and Edgington-Mitchell, D., "Impact of Coherence Decay on Wavepacket Models for Broadband Shock-Associated Noise in Supersonic Jets," *Journal of Fluid Mechanics*, Vol. 863, March 2019, pp. 969–993. https://doi.org/10.1017/jfm.2018.984

[24] Papamoschou, D., "Wavepacket Modeling of the Jet Noise Source," *International Journal of Aeroacoustics*, Vol. 17, Nos. 1–2, 2018, pp. 52–69. https://doi.org/10.1177/1475472X17743653

[25] Maia, I. A., Jordan, P., Cavalieri, A., and Jaunet, V., "Two-Point Wavepacket Modelling of Jet Noise," *Proceedings of the Royal Society of London, Series A: Mathematical and Physical Sciences*, Vol. 475, No. 2227, 2019, Paper 20190199. https://doi.org/10.1098/rspa.2019.0199

[26] Brès, G. A., and Lele, S. K., "Modelling of Jet Noise: A Perspective from Large-Eddy Simulations," *Philosophical Transactions of the Royal Society of London, Series A: Mathematical and Physical Sciences*, Vol. 377, No. 2159, 2019, Paper 20190081. https://doi.org/10.1098/rsta.2019.0081

[27] Brès, G. A., Ham, F. E., Nichols, J. W., and Lele, S. K., "Nozzle Wall Modeling in Unstructured Large Eddy Simulations for Hot Supersonic jet Predictions," AIAA Paper 2013-2142, 2013. https://doi.org/10.2514/6.2013-2142

[28] Brès, G. A., Jaunet, V., Le Rallic, M., Jordan, P., Towne, A., Schmidt, O., Colonius, T., Cavalieri, A. V., and Lele, S. K., "Large Eddy Simulation for Jet Noise: Azimuthal Decomposition and Intermittency of the Radiated Sound," AIAA Paper 2016-3050, 2016. https://doi.org/10.2514/6.2016-3050

[29] Schmidt, O. T., Towne, A., Rigas, G., Colonius, T., and Brès, G. A., "Spectral Analysis of Jet Turbulence," *Journal of Fluid Mechanics*, Vol. 855, Nov. 2018, pp. 953–982. https://doi.org/10.1017/jfm.2018.675

[30] Bertolotti, F., Herbert, T., and Spalart, P., "Linear and Nonlinear Stability of the Blasius Boundary Layer," *Journal of Fluid Mechanics*, Vol. 242, Sept. 1992, pp. 441–474. https://doi.org/10.1017/S0022112092002453

[31] Cavalieri, A. V., Rodrguez, D., Jordan, P., Colonius, T., and Gervais, Y., "Wavepackets in the Velocity Field of Turbulent Jets," *Journal of Fluid Mechanics*, Vol. 730, Sept. 2013, pp. 559–592. https://doi.org/10.1017/jfm.2013.346

[32] Gaster, M., "On the Effects of Boundary-Layer Growth on Flow Stability," *Journal of Fluid Mechanics*, Vol. 66, No. 3, 1974, pp. 465–480. https://doi.org/10.1017/S0022112074000310

[33] Crighton, D., and Gaster, M., "Stability of Slowly Diverging Jet Flow," *Journal of Fluid Mechanics*, Vol. 77, No. 2, 1976, pp. 397–413. https://doi.org/10.1017/S0022112076002176

[34] Gudmundsson, K., "Instability Wave Models of Turbulent Jets from Round and Serrated Nozzles," Ph.D. Thesis, California Inst. of Technology, Pasadena, CA, 2010. https://doi.org/10.7907/BQH9-G487

[35] Jiménez, J., "How Linear is Wall-Bounded Turbulence?" *Physics of Fluids*, Vol. 25, No. 11, 2013, Paper 110814. https://doi.org/10.1063/1.4819081

[36] Tissot, G., Zhang, M., Lajús, F. C., Cavalieri, A. V., and Jordan, P., "Sensitivity of Wavepackets in Jets to Nonlinear Effects: The Role of the Critical Layer," *Journal of Fluid Mechanics*, Vol. 811, Jan. 2017, pp. 95–137. https://doi.org/10.2514/6.2015-2218

[37] Towne, A., and Colonius, T., "One-Way Spatial Integration of Hyperbolic Equations," *Journal of Computational Physics*, Vol. 300, Nov. 2015, pp. 844–861. https://doi.org/10.1016/j.jcp.2015.08.015

[38] Towne, A., Rigas, G., and Colonius, T., "A Critical Assessment of the Parabolized Stability Equations," *Theoretical and Computational Fluid Dynamics*, Vol. 33, Nos. 3–4, 2019, pp. 359–382. https://doi.org/10.1007/s00162-019-00498-8

[39] Lesshafft, L., and Huerre, P., "Linear Impulse Response in Hot Round Jets," *Physics of Fluids*, Vol. 19, No. 2, 2007, Paper 024102. https://doi.org/10.1063/1.2437238

[40] Sinha, A., Rodrguez, D., Brès, G. A., and Colonius, T., "Wavepacket Models for Supersonic Jet Noise," *Journal of Fluid Mechanics*, Vol. 742, March 2014, pp. 71–95. https://doi.org/10.1017/jfm.2013.660

[41] Rodrguez, D., Cavalieri, A. V., Colonius, T., and Jordan, P., "A Study of Linear Wavepacket Models for Subsonic Turbulent Jets Using Local Eigenmode Decomposition of PIV Data," *European Journal of Mechanics-B/Fluids*, Vol. 49, Jan. 2015, pp. 308–321. https://doi.org/10.1016/j.euromechflu.2014.03.004

[42] Sasaki, K., Cavalieri, A. V., Jordan, P., Schmidt, O. T., Colonius, T., and Brès, G. A., "High-Frequency Wavepackets in Turbulent Jets," *Journal of Fluid Mechanics*, Vol. 830, Nov. 2017, p. R2. https://doi.org/10.1017/jfm.2017.659

[43] Cavalieri, A. V., Jordan, P., Colonius, T., and Gervais, Y., "Axisymmetric Superdirectivity in Subsonic Jets," *Journal of Fluid Mechanics*, Vol. 704, Aug. 2012, pp. 388–420.

[44] Towne, A., Cavalieri, A. V., Jordan, P., Colonius, T., Schmidt, O., Jaunet, V., and Brès, G. A., "Acoustic Resonance in the Potential Core of Subsonic Jets," *Journal of Fluid Mechanics*, Vol. 825, Aug. 2017, pp. 1113–1152. https://doi.org/10.1017/jfm.2017.346

[45] Schmidt, O., Towne, A., Colonius, T., Cavalieri, A., Jordan, P., and Brès, G., "Wavepackets and Trapped Acoustic Modes in a Turbulent Jet: Coherent Structure Eduction and Global Stability," *Journal of Fluid Mechanics*, Vol. 825, No. 1, 2017, pp. 1153–1181. https://doi.org/10.1017/jfm.2017.407